NANO LETTERS

Letter

pubs.acs.org/NanoLett

Growth of Adlayer Graphene on Cu Studied by Carbon Isotope Labeling

Qiongyu Li,[†] Harry Chou,[‡] Jin-Hui Zhong,[§] Jun-Yang Liu,[§] Andrei Dolocan,[‡] Junyan Zhang,[†] Yinghui Zhou,[†] Rodney S. Ruoff,[‡] Shanshan Chen,*[,†] and Weiwei Cai*[,†]

[†]Department of Physics, Laboratory of Nanoscale Condense Matter Physics, Xiamen University, Xiamen, China 361005

[‡]Department of Mechanical Engineering and the Materials Science and Engineering Program, The University of Texas, Austin, Texas 78712, United States

[§]Department of Chemistry, College of Chemistry and Chemical Engineering, Xiamen University, Xiamen, 361005, China

ABSTRACT: The growth of bilayer and multilayer graphene on copper foils was studied by isotopic labeling of the methane precursor. Isotope-labeled graphene films were characterized by micro-Raman mapping and time-of-flight secondary ion mass spectrometry. Our investigation shows that during growth at high temperature, the adlayers formed simultaneously and beneath the top, continuous layer of graphene and the Cu substrate. Additionally, the adlayers share the same nucleation center and all adlayers nucleating in one place have the same edge termination. These results suggest that adlayer growth proceeds by catalytic decomposition of methane (or CH_x, $x < 4$) trapped in a "nano-chemical vapor deposition" chamber between the first layer and the substrate. On the basis of these results, submillimeter bilayer graphene was synthesized by applying a much lower growth rate.

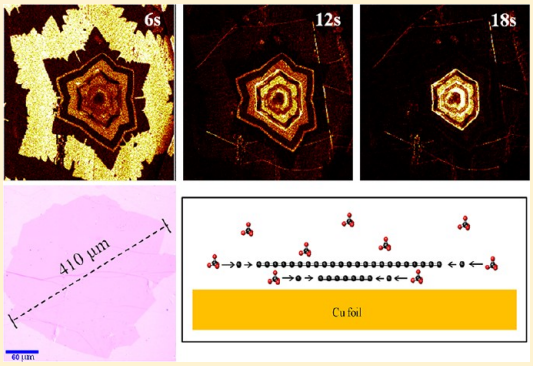

KEYWORDS: *Graphene, adlayer, isotope-labeling, micro-Raman mapping, TOF SIMS*

Chemical vapor deposition (CVD) techniques have been used to grow high quality monolayer graphene films on various metal substrates,[1−4] achieving large area coverage up to 30 in. along the diagonal.[5] CVD graphene can have carrier mobility values in excess of 7100 $cm^2/(V\ s)$ at room temperature,[6] which is close to the results on SiO_2/Si with graphene exfoliated from HOPG or kish graphite. The high carrier mobility and size scalability make CVD graphene a promising material for applications such as integrated high frequency electronics. However, monolayer graphene has a unique zero-bandgap dispersion relation,[7] limiting its potential as a logic switch or for memory. In AB stacked bilayer graphene, a band gap can be opened and field-effect transistors with dual gates have been fabricated.[8]

Recently, several groups, including ours, have reported the growth of bilayer graphene on Cu[9,10] and Cu−Ni alloy[11] substrates via CVD. However, the formation mechanism of adlayer regions is not well understood or even controversial.[12,13] Nie et al. report that the underlayer formation mechanism (~10 μm second layer under the first layer) facilitates the synthesis of uniform single-layer graphene but presents challenges for growing large area bilayer films by ambient pressure CVD.[12] Kalbac et al. evaluate the second layer to be on top of the first layer through hydrogen etching process by low pressure CVD that presents the same challenge for growing large area bilayer graphene.[13] We here report a study of the mechanism of adlayer graphene growth by using isotopic labeling of the methane precursor during synthesis. The stacking order of the bilayer graphene and multilayer graphene is clearly depicted through Micro Raman and Time of Flight Secondary Ion Mass Spectrometry(TOF-SIMS) mapping. Moreover, by careful control of the growth rate, submillimeter uniform bilayer graphene could be achieved under the first layer.

High-quality multilayer graphene films were synthesized by CVD on the interior surface of Cu foil enclosures.[14] The base pressure of the CVD chamber was 1.5 mTorr. After annealing in 1 sccm H_2 (99% pure) for 30 min at 1030 °C in a quartz tube furnace, methane or isotopically labeled methane was introduced sequentially, first 1 sccm $^{12}CH_4$ (99% pure) for 12 min, then $^{13}CH_4$ (99.95% pure) for 12 min, and so on, for 108 min total time at a total pressure of 49 mTorr.[3] For submillimeter bilayer graphene growth, 0.1 sccm $^{12}CH_4$ (99% pure) and 10 sccm H_2 was introduced at 1030 °C for 3h at a total pressure of 150 mTorr. After growth, the graphene films were transferred onto pieces of Si wafers with a 300 nm thick SiO_2 overlayer, as described previously.[15,16] Figure 1a shows an optical micrograph of the graphene transferred onto the SiO_2/Si wafer. The variation of color contrast in the optical micrograph clearly indicates this particular graphene grain

Received: October 22, 2012
Revised: December 19, 2012

   dx.doi.org/10.1021/nl303879k | *Nano Lett.* XXXX, XXX, XXX−XXX

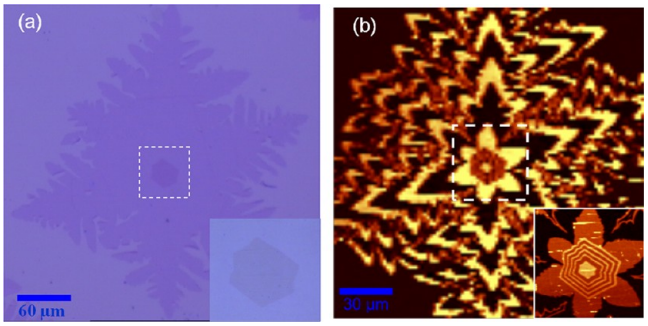

Figure 1. Bilayer graphene on a SiO_2/Si substrate. (a) Optical image of one graphene grain with bilayer on a 300 nm SiO_2/Si wafer. Inset shows the enlarged figure from the dotted square. (b) Raman map of G_{12} band intensity (1560−1600 cm^{-1}) from the same graphene grain in (a). The inset in (b) shows the detail of the bilayer region.

consists of single-layer regions and bilayer regions which was marked by the white dotted square and shown in the inset.[17]

Micro-Raman mapping was used to study the distinctive phonon mode signatures of the isotope-engineered samples, and provided important insights into the mechanism of growth of adlayer graphene. Specific Raman bands will be labeled as D_{13} (1300 cm^{-1}), G_{13} (1520 cm^{-1}), $2D_{13}$ (2550 cm^{-1}) and D_{12} (1350 cm^{-1}), G_{12} (1580 cm^{-1}), $2D_{12}$ (2680 cm^{-1}), which correspond to the D, G, and 2D band of ^{13}C and ^{12}C graphene, respectively.[3,18] Figure 1b shows the Raman map of the G_{12} band acquired from the graphene film shown in Figure 1a. Because of the nature of graphene growth on Cu, the sequential dosing of non-labeled and then ^{13}C-labeled methane yields isotopically distinct graphene regions in the graphene film.[3] It is notable that the adlayer graphene maintains isotopically distinct regions that "track" those in the top layer (the ordering of layers is proven below), albeit, with narrower bands that reflect the significantly slower growth rate of the adlayer. We observed that the adlayer growth started at the same nucleation center and terminated after the same number of "rings" as the first layer.

In an attempt to assign the stacking order of the bilayer graphene, the transferred graphene grain was exposed for 5 s to an O_2 plasma in an attempt to generate defects on the upper graphene layer to distinguish it from the layers beneath it. Figure 2a,b shows a Raman map of the G_{12} band before and after exposure to the O_2 plasma, respectively. Figure 2c,d shows a schematic of the cross-section view from the white dotted line marked in Figure 2a,b, respectively. Figure 2e,f shows Raman spectra taken from positions where the adlayer is ^{13}C graphene and the top layer is ^{12}C graphene (labeled in Figure 2c,d by the arrow, respectively). Prior to the short time exposure to the O_2 plasma, the Raman data (Figure 2e) shows the characteristic bands for G_{13}, G_{12}, $2D_{13}$, and $2D_{12}$, which indicate the presence of bilayer graphene. After the 5 s O_2 plasma exposure, the Raman spectrum shows an additional resonance peak associated only with the defect band of ^{12}C (D_{12}, ~1350

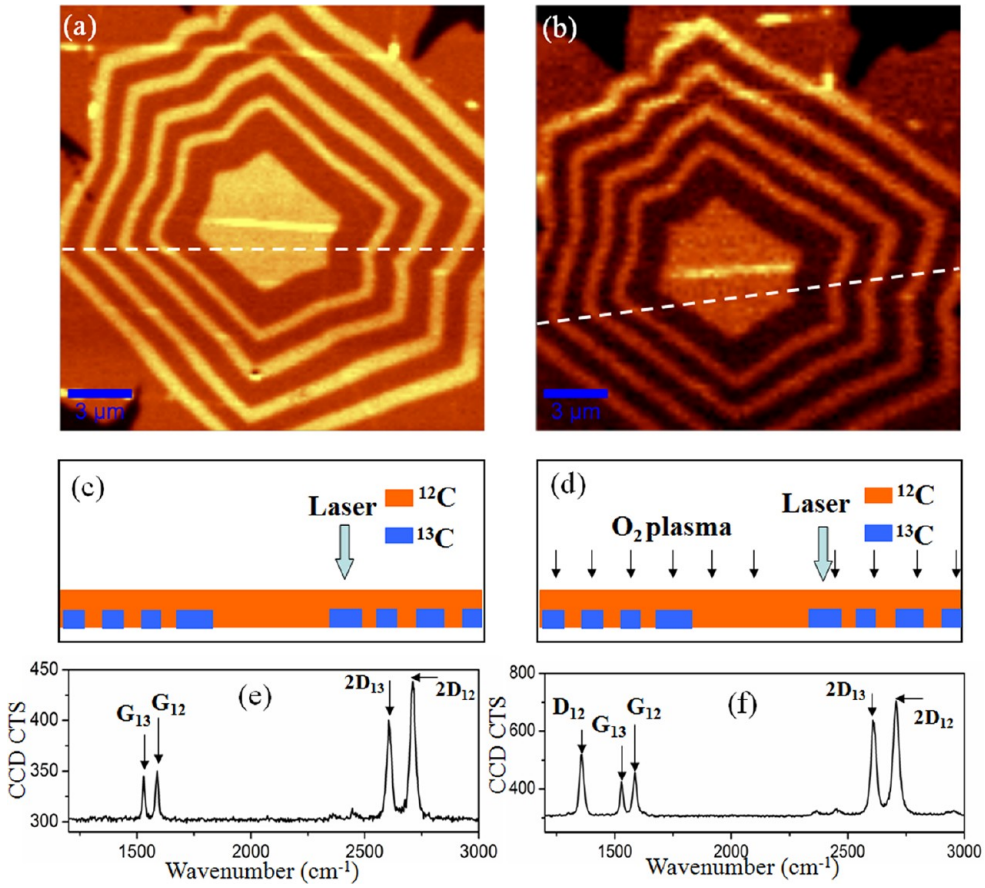

Figure 2. Raman of isotopically labeled bilayer graphene before and after oxygen plasma etching. (a,b) Raman map of the G_{12} band intensity (1560−1600 cm^{-1}) from the transferred graphene before (a) and after (b) oxygen plasma etching. (c,d) Cross-section of the graphene layers at the position marked in (a,b) by a white line, respectively. (e,f) Raman spectra taken from the positions indicated in (c,d) by arrows, respectively.

dx.doi.org/10.1021/nl303879k | *Nano Lett.* XXXX, XXX, XXX−XXX

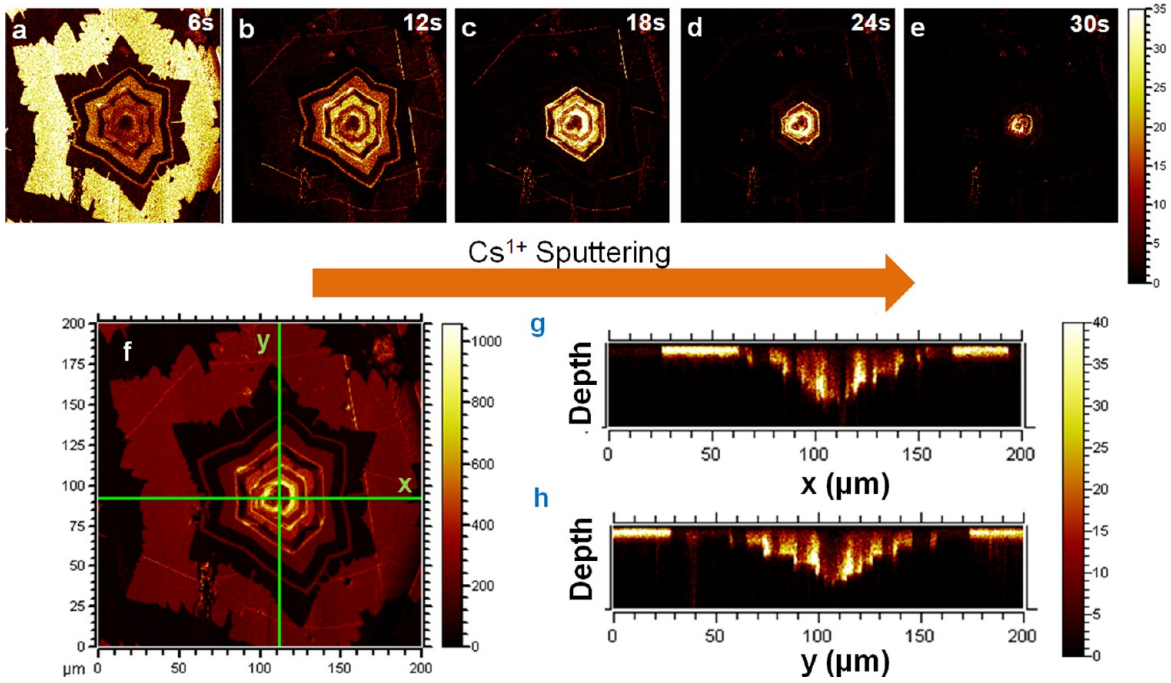

Figure 3. TOF SIMS mapping (200 × 200 μm^2) of isotopically labeled multilayer graphene on Cu foil. (a–e) The ^{12}C isotope distribution images of graphene by TOF SIMS after 6 s (a), 12 s (b), 18 s (c), 24 s (d), and 30 s (e) 1 kV Cs^{1+} ion beam sputter. (f) The overall sum image of 36 total images. (g,h) The cross-section views of ^{12}C graphene from the marked *x* (g) and *y* (h) lines in (f). The color scale represents secondary ion intensity.

cm^{-1}). This indicates that only the ^{12}C graphene layer was influenced by the short time exposure to the O_2 plasma and therefore that the ^{12}C graphene layer was indeed the outermost layer. If the opposite were true with the ^{13}C layer on top of the ^{12}C layer, a ^{13}C defect band would have instead been detected (D_{13}, ~1300 cm^{-1}) after exposure to the O_2 plasma. Since the stacking order of the film is not changed during the transfer process, this result clearly shows that the adlayer graphene formed below the first layer on the Cu substrate.

In order to further test this conclusion on the multilayer graphene grains, we performed TOF-SIMS (ION-TOF GmbH TOF.SIMS5) depth profile analysis to image the sample isotope distribution and the stacking order on the as-grown multilayer graphene on Cu substrates. This technique allowed fine control over the removal of individual atomic layers as well as achieving high sensitivity (down to parts-per-billion) and mass resolution ($m/\delta m > 7000$) to all chemical components in the sample. A Cs^{1+} ion beam (1 kV energy) was used for layer removal while the sample composition was mapped in Burst Alignment (BA) mode (i.e., high lateral resolution, about 200 nm) by a 30 kV Bi^{1+} ion beam.

With the ability to easily distinguish between grains along the surface and between layers into the surface, the stacking order of the adlayers was revealed. The order of layer growth was determined by noting the width of the isotope-labeled bands attributed to the change in the growth rate from the first layer to the second. The ^{12}C and ^{13}C secondary ion intensities show that smaller adlayers with narrower bands were revealed as the outer layers were removed. The top-down ^{12}C TOF-SIMS maps in Figure 3(a–e) clearly show that the graphene was removed layer by layer (about 6 s of Cs^+ sputtering per layer). Because of some adsorbed contamination on the surface due to sample handling and exposure to air, a few seconds of Cs^+ sputtering were needed before the outermost graphene layer was fully revealed (which here is normal graphene, i.e., predominantly ^{12}C). After 6 s of Cs^+ sputtering, we begin to see a clear image of this first layer (Figure 3a), and as the sputtering continues the second layer (Figure 3b) takes form. As the outer layers are removed, still more adlayers are detected underneath. While the intensity of the adlayer signal clearly shows they reside beneath the initial monolayer, their shape can be distinguished even at the outermost layer. This may be explained by the cascade collisions inherent in all SIMS analysis.[19] The overall sum image combining all the layers is shown in Figure 3f, where we could see the presence of edge terminations from all the adlayers. The cross-section view (Figure 3g,h) from the marked lines in Figure 3f clearly show that the adlayers grow beneath the first monolayer of graphene.

On the basis of these observations, we find that graphene adlayers form between the first layer and the substrate. The maps of isotope distribution from both micro-Raman mapping and TOF-SIMS show that the adlayer graphene grows simultaneously with the first layer, showing the same number of "bands" corresponding to the dosing sequence of $^{12}CH_4$ and $^{13}CH_4$. Also, it is noted that the adlayer graphene terminated simultaneously with the first layer as both layers contain the same number of bands. These results suggest that adlayers and monolayers grow by a similar self-limited surface deposition process.[1] This self-limited process is distinct from the segregation process that is observed in Ir(111) and Ru(0001), where later graphene layers also form underneath the first layer.[20,21]

Given this evidence, a mechanism for adlayer graphene growth, which reflects the similarity to monolayer graphene growth, can be proposed. Our previous results conclusively show that the first layer graphene grows by a C surface nucleation and surface-catalyzed process.[1] Because of the extremely strong and favorable C–C bond, C is captured

dx.doi.org/10.1021/nl303879k | *Nano Lett.* XXXX, XXX, XXX–XXX

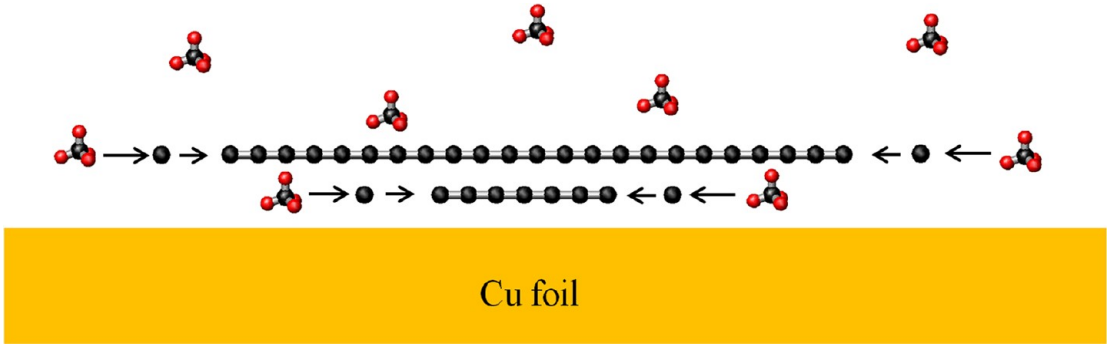

Figure 4. Schematic of growth mechanism of the adlayer graphene.

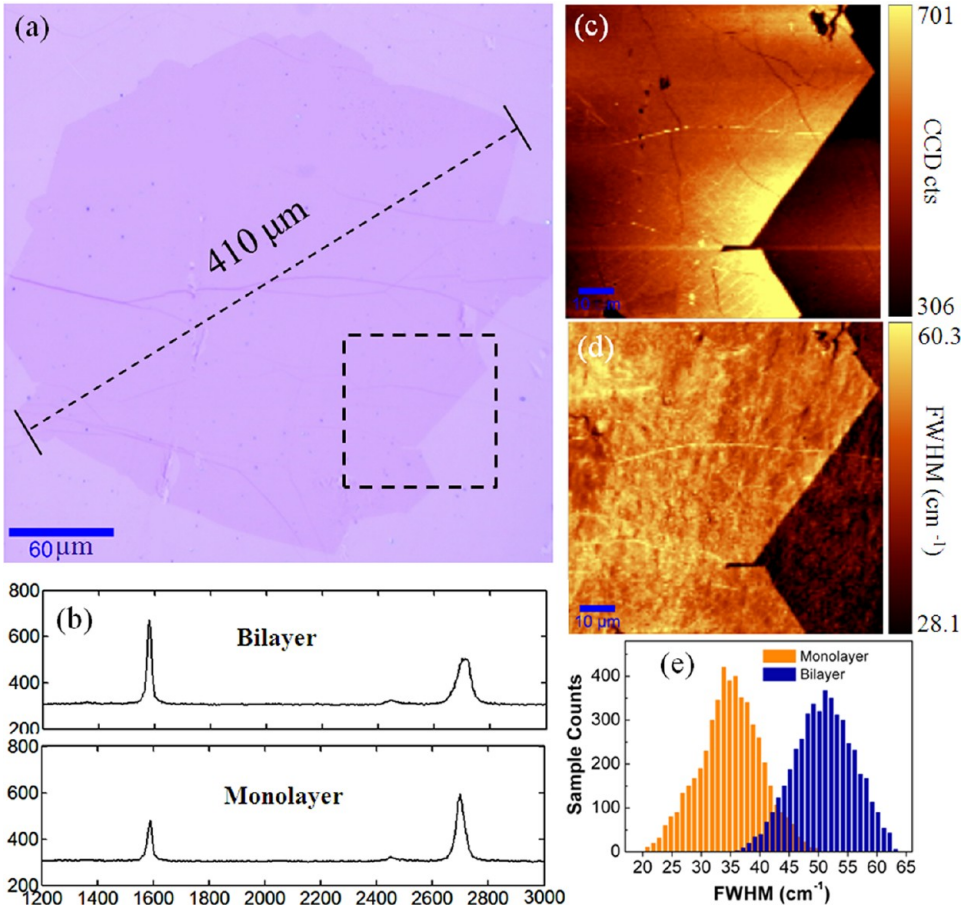

Figure 5. Submillimeter bilayer graphene on a SiO_2/Si substrate. (a) Optical image of the graphene grain transferred onto the 300 nm SiO_2/Si substrate. (b) Typical Raman spectra taken on the bilayer and the monolayer graphene area in (a), respectively. (c,d) Raman G band map (1560−1600 cm^{-1}) and fwhm of 2D band map (2630−2730 cm^{-1}) from the dotted square in (a). (e) Histogram of the fwhm of Raman 2D band of monolayer and bilayer graphene.

once it diffuses to the edge of the first layer graphene grain. A large Ehrlich-Schwoebel barrier[22] can prevent C from diffusing to either the outer surface of the first layer or the interfaces between the first layer and Cu. However, it has been observed that many gas molecules readily diffuse into the interface between graphene and its metal substrate.[19,23] The presence of molecules in the interface is attributed to the weak interaction between graphene and its substrate.[23] The dissociation of methane from its initial state (as an adsorbed CH_4 molecule) to the final product (atomic carbon atom) on Cu surfaces is understood to be a highly endothermic process. This suggests that three intermediates (CH_3, CH_2, and CH) exist at the Cu surface in addition to the atomic carbon atoms.[22] As shown in Figure 4, we propose that the growth mechanism of adlayer graphene is the catalytic decomposition of CH_x (x is possibly 0, 1, 2, 3, or 4, or combinations thereof ≤ 4), whose components diffuse into the interface between the first layer and the substrate. This limited space in the interface will form a "nano-CVD" chamber. The extreme physical confines in the nano-CVD chamber result in a lower partial pressure of CH_x, which manifests in a decreased growth rate and improved the crystal quality of the adlayer graphene. These graphene grains tend to show hexagonal shapes, rather than the flowerlike shapes that are commonly observed for the first layer. It is very likely that

dx.doi.org/10.1021/nl303879k | *Nano Lett.* XXXX, XXX, XXX−XXX

with a much slower growth rate (for example, the adlayer in Figure 1 grows at a rate about two orders of magnitude slower than the first layer), the active carbon species in the nano-CVD diffuses slowly with respect to the relaxation time and with an adequate activation energy will form the more thermodynamically favorable hexagonal graphene grain shape at the high growth temperature (1030 °C).

Since intercalation takes place through open channels at the edges of the first graphene layer,[23] the adlayer graphene growth terminates when the first layer grains merge together. When neighboring grains merge, the open channels are effectively shut, terminating the first layer growth and adlayer growth simultaneously.

The study of the adlayer graphene growth on Cu suggests an approach for synthesis of large area bilayer graphene by using slower growth rate compared to previous monolayer graphene synthesis.[1] A relative low methane ($^{12}CH_4$ (99% pure)) flow rate (~ 0.1 sccm) was used, by which the first layer grains were not able to merge together without a two step growth involving by increased methane flow or pressure.[24] The inability to form a complete monolayer favors the continuous growth of the adlayer. Figure 5a shows an optical micrograph of a portion of a graphene grain transferred onto the SiO_2/Si substrate. Color contrast in this image indicates that after 3 h growth large area uniform bilayer graphene grains up to 0.41 mm along the diagonal direction were obtained. A typical Raman spectrum (Figure 5a) from the bilayer area in Figure 5b shows ~1.5 I_G/I_{2D} and a fwhm of 2D band of ~51 cm^{-1}, suggesting the strong interlayer coupling of the bilayer graphene. Figure 5c,d shows a Raman map of the G_{12} band (1580 cm^{-1}) and fwhm of $2D_{12}$ band (2680 cm^{-1}) taken from the rectangle area in Figure 5a, which consists of monolayer and bilayer graphene. The uniformity of the Raman G band confirms the uniformity of the graphene thickness, while the fwhm map indicates the bilayer graphene obtained here is homogeneously A-B stacked. In addition, from the histogram of the fwhm of Raman 2D band (Figure 5e), the average values of the obtained monolayer and bilayer graphene are determined to be 34 ± 3 and 52 ± 3 cm^{-1}, respectively.

The methods and results presented in this paper show that during high temperature growth adlayer graphene forms between the first graphene layer and its substrate. The adlayers form at the same initial nucleation centers and terminate growth simultaneously with the first layer. We propose that the growth mechanism of adlayer graphene is the catalytic decomposition of methane or CH_x ($x \leq 4$) in nano-CVD chambers defined by the first graphene layer and its substrate. On the basis of these results, submillimeter bilayer graphene was synthesized by using slower growth rate compared to previous monolayer graphene synthesis.

AUTHOR INFORMATION

Corresponding Author

*E-mail: (W.C.) wwcai@xmu.edu.cn; (S.C.) sschen@xmu.edu.cn.

Notes

The authors declare no competing financial interest.

ACKNOWLEDGMENTS

We appreciate support from the National Natural Science Foundation of China through Grants 91123009, 10975115 and Natural Science Foundation of Fujian Province of China (No. 2012J06002). H.C., S.C., and R.S.R. were supported by the SWAN NRI and the Office of Naval Research. We also acknowledge the TOF-SIMS facility (NSF Grant DMR-0923096), part of and the Texas Materials Institute at the University of Texas at Austin for the TOF-SIMS data acquisition and interpretation.

REFERENCES

(1) Li, X. S.; Cai, W. W.; An, J. H.; Kim, S.; Nah, J.; Yang, D. X.; Piner, R.; Velamakanni, A.; Jung, I.; Tutuc, E.; Banerjee, S. K.; Colombo, L.; Ruoff, R. S. *Science* **2009**, *324* (5932), 1312−1314.

(2) Kim, K. S.; Zhao, Y.; Jang, H.; Lee, S. Y.; Kim, J. M.; Ahn, J. H.; Kim, P.; Choi, J. Y.; Hong, B. H. *Nature* **2009**, *457* (7230), 706−710.

(3) Li, X. S.; Cai, W. W.; Colombo, L.; Ruoff, R. S. *Nano Lett.* **2009**, *9* (12), 4268−4272.

(4) Reina, A.; Jia, X. T.; Ho, J.; Nezich, D.; Son, H. B.; Bulovic, V.; Dresselhaus, M. S.; Kong, J. *Nano Lett.* **2009**, *9* (1), 30−35.

(5) Bae, S.; Kim, H.; Lee, Y.; Xu, X. F.; Park, J. S.; Zheng, Y.; Balakrishnan, J.; Lei, T.; Kim, H. R.; Song, Y. I.; Kim, Y. J.; Kim, K. S.; Ozyilmaz, B.; Ahn, J. H.; Hong, B. H.; Iijima, S. *Nat. Nanotechnol.* **2010**, *5* (8), 574−578.

(6) Gao, L. B.; Ren, W. C.; Xu, H. L.; Jin, L.; Wang, Z. X.; Ma, T.; Ma, L. P.; Zhang, Z. Y.; Fu, Q.; Peng, L. M.; Bao, X. H.; Cheng, H. M. *Nat. Commun.* **2012**, *3*, 699.

(7) Novoselov, K. S.; Geim, A. K.; Morozov, S. V.; Jiang, D.; Zhang, Y.; Dubonos, S. V.; Grigorieva, I. V.; Firsov, A. A. *Science* **2004**, *306* (5696), 666−669.

(8) Ohta, T.; Bostwick, A.; Seyller, T.; Horn, K.; Rotenberg, E. *Science* **2006**, *313* (5789), 951−954.

(9) Yan, K.; Peng, H. L.; Zhou, Y.; Li, H.; Liu, Z. F. *Nano Lett.* **2011**, *11* (3), 1106−1110.

(10) Lee, S.; Lee, K.; Zhong, Z. H. *Nano Lett.* **2010**, *10* (11), 4702−4707.

(11) Chen, S. S.; Cai, W. W.; Piner, R. D.; Suk, J. W.; Wu, Y. P.; Ren, Y. J.; Kang, J. Y.; Ruoff, R. S. *Nano Lett.* **2011**, *11* (9), 3519−3525.

(12) Nie, S.; Wu, W.; Xing, S. R.; Yu, Q. K.; Bao, J. M.; Pei, S. S.; McCarty, K. F. *New J. Phys.* **2012**, *14*, 093028.

(13) Kalbac, M.; Frank, O.; Kavan, L. *Carbon* **2012**, *50*, 3682−3687.

(14) Li, X. S.; Magnuson, C. W.; Venugopal, A.; Tromp, R. M.; Hannon, J. B.; Vogel, E. M.; Colombo, L.; Ruoff, R. S. *J. Am. Chem. Soc.* **2011**, *133* (9), 2816−2819.

(15) Chen, S.; Wu, Q.; Mishra, C.; Kang, J.; Zhang, H.; Cho, K.; Cai, W.; Balandin, A. A.; Ruoff, R. S. *Nat. Mater.* **2012**, *11* (3), 203−207.

(16) Li, X. S.; Zhu, Y. W.; Cai, W. W.; Borysiak, M.; Han, B. Y.; Chen, D.; Piner, R. D.; Colombo, L.; Ruoff, R. S. *Nano Lett.* **2009**, *9* (12), 4359−4363.

(17) Blake, P.; Hill, E. W.; Neto, A. H. C.; Novoselov, K. S.; Jiang, D.; Yang, R.; Booth, T. J.; Geim, A. K. *Appl. Phys. Lett.* **2007**, *91* (6), 063124.

(18) Cai, W. W.; Piner, R. D.; Stadermann, F. J.; Park, S.; Shaibat, M. A.; Ishii, Y.; Yang, D. X.; Velamakanni, A.; An, S. J.; Stoller, M.; An, J. H.; Chen, D. M.; Ruoff, R. S. *Science* **2008**, *321* (5897), 1815−1817.

(19) Starodub, E.; Bartelt, N. C.; McCarty, K. F. *J. Phys. Chem. C* **2010**, *114* (11), 5134−5140.

(20) Nie, S.; Walter, A. L.; Bartelt, N. C.; Starodub, E.; Bostwick, A.; Rotenberg, E.; McCarty, K. F. *ACS Nano* **2011**, *5* (3), 2298−2306.

(21) Cui, Y.; Fu, Q.; Bao, X. H. *Phys. Chem. Chem. Phys.* **2010**, *12* (19), 5053−5057.

(22) Zhang, W. H.; Wu, P.; Li, Z. Y.; Yang, J. L. *J. Phys. Chem. C* **2011**, *115* (36), 17782−17787.

(23) Mu, R. T.; Fu, Q.; Jin, L.; Yu, L.; Fang, G. Z.; Tan, D. L.; Bao, X. H. *Angew. Chem., Int. Ed.* **2012**, *51* (20), 4856−4859.

(24) Li, X. S.; Magnuson, C. W.; Venugopal, A.; An, J.; Suk, J. W.; Han, B. Y.; Borysiak, M.; Cai, W. W.; Velamakanni, A.; Zhu, Y. W.; Fu, L. F.; Vogel, E. M.; Voelkl, E.; Colombo, L.; Ruoff, R. S. *Nano Lett.* **2010**, *10* (11), 4328−4334.